

Solution-Phase Synthesis of Highly Conductive Tungsten Diselenide Nanosheets

Priscilla D. Antunez, David H. Webber, and Richard L. Brutchey*

Department of Chemistry and the Center for Energy Nanoscience and Technology, University of Southern California, Los Angeles, California 90089-0744, United States

S Supporting Information

KEYWORDS: tungsten selenide, WSe_2 , nanosheet, transition metal dichalcogenide, layered material, conductivity

Early transition metal dichalcogenides are an important class of layered materials that have been used for hydrogen storage, transistors, lubricants, catalysis, capacitors, batteries, and photovoltaic devices.¹ The structure of transition metal dichalcogenides consists of repeating crystalline layers, which are responsible for their 2D anisotropic physical properties. Notable properties of transition metal dichalcogenides include superconducting behavior in $NbSe_2$ and TaS_2 ² and the observation of ultralow thermal conductivities ($0.05 \text{ W m}^{-1} \text{ K}^{-1}$) in disordered WSe_2 crystals.³ In the nanoscale regime, transition metal dichalcogenides have recently been shown to exhibit properties that make them particularly interesting when compared to bulk material. For example, MoS_2 nanotubes are more air stable and exhibit greater loading capacities of Li than in the bulk.⁴ Moreover, certain transition metal dichalcogenides have been shown to change from indirect to direct band gap semiconductors when isolated as single layers.⁵

Bulk tungsten diselenide (WSe_2) is an indirect semiconductor that can be doped to generate a *p*- or *n*-type type material.⁶ Bulk WSe_2 possesses a band gap of $E_{g,indir} = 1.2 \text{ eV}$,⁷ a high absorption coefficient, and high photostability.^{6a} In addition, its incorporation into photoelectrochemical devices has resulted in conversion efficiencies up to 17% ($J_{SC} = 38 \text{ mA cm}^{-2}$).⁸ Bulk WSe_2 exhibits hole carrier concentrations of $3.88 \times 10^{17} \text{ cm}^{-3}$ and highly anisotropic conductivities that range between 0.7 and 6.0 S cm^{-1} for in-plane measurements.⁹ Tungsten diselenide crystallizes in Se–W–Se layers where tungsten coordinates through strong covalent-ionic bonds (ca. 13% fractional ionic character) to six selenium atoms in a trigonal prismatic geometry.¹⁰ Variations in layer stacking result in different polytypes; the 2H- WSe_2 polytype refers to the two layers and the hexagonal structure represented in one unit cell, corresponding to the hexagonal molybdenite structure ($P6_3/mmc$).¹¹

Traditional methods to prepare WSe_2 include sputtering, chemical vapor transport, solid-state reactions, and electro-deposition;¹² however, there have been very few reports of solution-phase syntheses of colloidal WSe_2 nanostructures. In 2000, Huang et al. synthesized 4–7 nm WSe_2 nanoparticles by the reaction of H_2Se with WCl_4 dissolved in a ternary tridodecylmethylammonium iodide/hexane/octane inverse micelle solution.¹³ In 2004, Duphil et al. synthesized WSe_2 nanoparticles by the reaction of elemental Se with $W(CO)_6$

dissolved in *p*-xylene at $140 \text{ }^\circ\text{C}$ for several hours.¹⁴ The resulting 10–30 nm nanoparticles were then annealed at $550 \text{ }^\circ\text{C}$, with X-ray diffraction (XRD) patterns revealing crystalline tungsten oxide impurities. Herein, we present the first report of a facile solution-phase synthesis of colloidal WSe_2 nanosheets.

Diorganodichalcogenides have proven to be useful chalcogen sources for the facile solution-phase synthesis of colloidal semiconductor nanocrystals.¹⁵ The synthesis of WSe_2 nanosheets was achieved by the injection of $185 \mu\text{L}$ (0.92 mmol) di-*tert*-butyl diselenide ($t\text{-Bu}_2\text{Se}_2$) into a solution of 150 mg (0.46 mmol) WCl_4 in 25 mL of dodecylamine at $150 \text{ }^\circ\text{C}$ under nitrogen. The solution was then heated to $225 \text{ }^\circ\text{C}$ and held at this temperature for 6 h prior to quenching. Tetra-*n*-octylammonium bromide (TOAB) was added during the workup to prevent agglomeration of the nanosheets, following an adapted version of a previously published method.¹⁶ The final washed product was highly dispersible in tetramethylurea (TMU) and 1,2-dichlorobenzene, forming colloidal suspensions that were stable over the course of several months. Although dispersions in toluene were not very colloidal stable, they produce visually smooth films upon drop casting that were used throughout this study unless otherwise noted. The omission of TOAB during the workup procedure yielded macroscopic, scroll-like pieces of WSe_2 instead of films upon deposition. The synthesis was reproducible and yielded ca. 150 mg of WSe_2 . On the basis of tungsten, the WSe_2 yield was $\sim 90\%$, taking into account the 12% organic content observed by thermogravimetric analysis (TGA) (see Supporting Information, Figure S1). Differential scanning calorimetry (DSC) corroborated the endothermic loss of organic material between 250 and $475 \text{ }^\circ\text{C}$ (see Supporting Information, Figure S1).

Powder X-ray diffraction patterns of annealed and unannealed WSe_2 nanosheets both appear to be phase pure without any crystalline tungsten oxide impurities observed in the $20\text{--}30^\circ 2\theta$ range (Figure 1). Despite the air stability of the product, tungsten oxide impurities were readily obtained unless strictly anaerobic conditions were employed during both the synthesis and annealing steps. The three XRD patterns in Figure 1

Received: March 10, 2013

Revised: May 24, 2013

Published: May 30, 2013

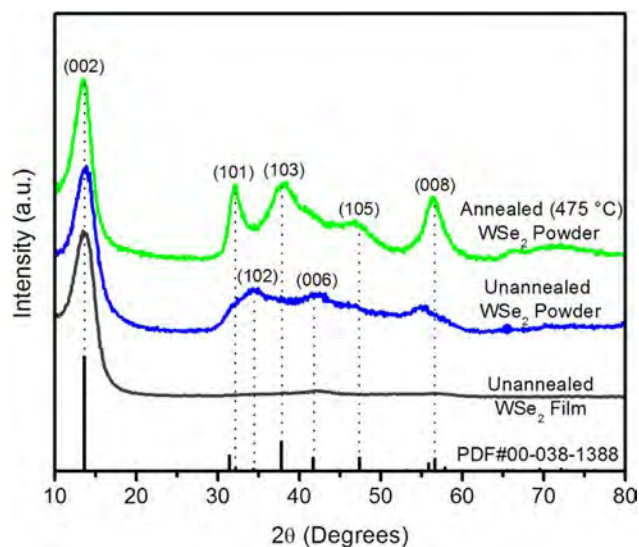


Figure 1. Film and powder XRD patterns of WSe₂ nanosheets before and after annealing at 475 °C.

display a 100% intensity peak ($2\theta = 13.5^\circ$) indexed to the (002) reflection of the 2H-WSe₂ phase (JCPDS no. 00-038-1388).¹⁷ Unannealed, drop-cast films displayed the (002) reflection as the prominent diffraction peak along with very small peaks at ca. $2\theta = 42$ and 57° that correspond to the (006) and (008) reflections, respectively, suggesting a strong preference for [001] orientation. Powdering the sample to reduce preferred orientation effects resulted in a diffraction pattern showing very broad diffraction peaks between $2\theta = 30$ – 60° , including the (102) reflection. Upon annealing the powdered WSe₂ nanosheets in a tube furnace for 5 min (475 °C under flowing nitrogen), additional peaks became prominent; these were indexed to the (101), (103), and (105) lattice planes. To corroborate the X-ray structure data, Raman spectra of the annealed and unannealed WSe₂ films were collected. The Raman spectra of annealed and unannealed WSe₂ films both reveal a characteristic band at ca. 257 cm^{-1} that can be assigned to the almost degenerate E_{2g}^1 and A_{1g} Raman active modes of WSe₂, while the band at ca. 179 cm^{-1} was assigned to the E_{1g} mode, indicative of the 2H-WSe₂ structure (see Supporting Information, Figure S2).¹⁸ The unassigned peaks at ca. 127 and 319 cm^{-1} have been observed in WSe₂ single crystals¹⁹ and are also present in the Raman spectrum of “as bought” WSe₂ powder (Alfa Aesar).

Scanning electron microscope energy-dispersive X-ray spectroscopy (SEM-EDX) and ion coupled plasma atomic emission spectrometry (ICP-AES) were used to analyze the elemental composition of the resulting WSe₂ nanosheets. Analysis of randomly selected areas gave an average W/Se composition of 1:2.0 for the unannealed material and a 1:1.8 for the annealed material (see the Supporting Information, Figure S3). ICP-AES results were in close agreement, giving an average W/Se composition of 1:2.3 for the unannealed WSe₂ nanosheets.

Transmission electron microscope (TEM) analysis of the product revealed the nanosheet morphology of the WSe₂. Samples drop-cast from toluene showed some agglomerates with nano-onion structures and sheets with extended alignment (Figure 2b; Supporting Information, Figure S4), while those dried from TMU showed less extensive alignment (Figure 2a; Supporting Information, Figure S5). Individual thin sheets of various sizes were found around the agglomerates (see

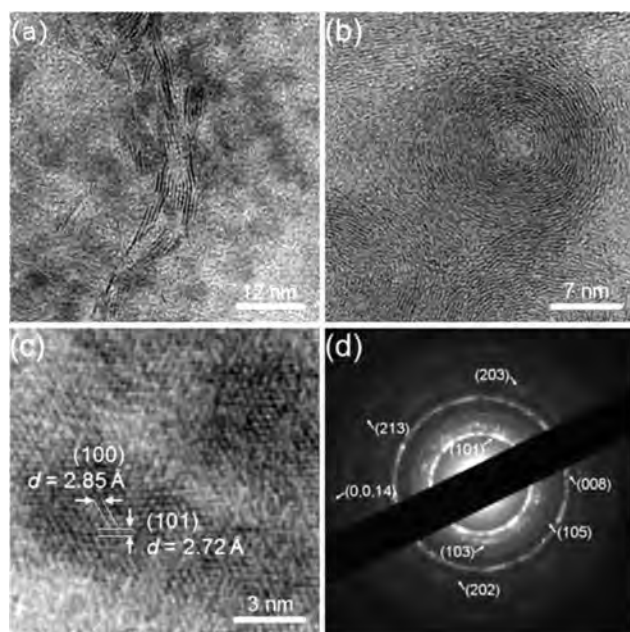


Figure 2. HR-TEM images of (a) typical WSe₂ nanosheets dried from TMU, (b) nano-onion structures of WSe₂ nanosheets dried from toluene, and (c) lattice fringes with interplanar spacings of $d = 2.85$ and 2.72 \AA . (d) SAED pattern of annealed WSe₂ nanosheets indexed to 2H-WSe₂.

Supporting Information, Figure S6). A high resolution TEM (HR-TEM) image of a nanosheet displaying its (100) and (101) lattice planes ($d = 2.85$ and 2.72 \AA , respectively) is shown in Figure 2c. Although lattice fringes were observed throughout the unannealed WSe₂ nanosheets, only a few diffuse rings were observed by selected area electron diffraction (SAED; see Supporting Information, Figure S7). This suggests that the unannealed WSe₂ nanosheets are weakly crystalline, as the powder XRD data also suggests. In contrast, more intense diffraction was observed in the SAED pattern of the annealed WSe₂ nanosheets; these were indexed in agreement with the XRD results (Figure 2d).

The electrical transport properties of the solution-processed WSe₂ nanosheets were also studied. Figure 3 shows the

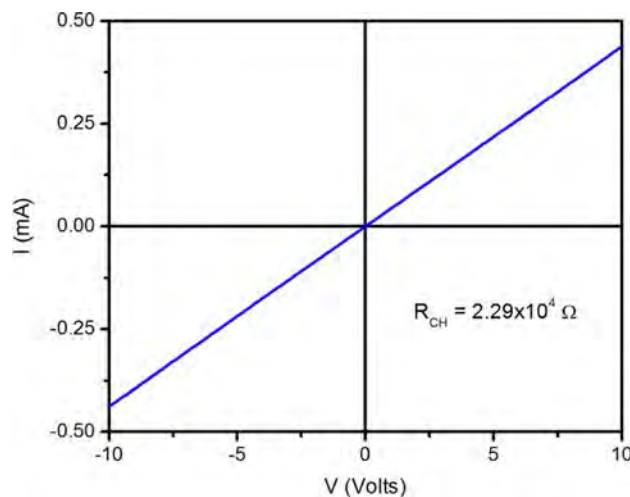


Figure 3. Room temperature two-point I – V measurements of an unannealed WSe₂ film using a $0.85\text{ mm} \times 5.87\text{ mm} \times 75\text{ nm}$ channel.

current–voltage (I – V) characteristics of an unannealed WSe_2 film that was solution deposited between two aluminum electrodes. The material was simply drop-cast from toluene and allowed to dry in air to give [001] oriented films (vide supra). The room temperature two-point I – V data of the unannealed films were collected using two types of devices with different channel dimensions to verify the measured conductivity values. Both unannealed and annealed films exhibited linear I – V behavior, representative of ohmic contact between the WSe_2 nanosheets and the Al electrodes. Eight devices from three different batches of WSe_2 nanosheets synthesized using identical conditions gave an average conductivity of $0.6 \pm 0.4 \text{ S cm}^{-1}$, which is in the same order of magnitude as WSe_2 single crystals (0.7 S cm^{-1})^{9a} and highly conductive WSe_2 thin films (0.1 S cm^{-1}).^{12a} Annealing the devices ($475 \text{ }^\circ\text{C}$) increased the average conductivity by 2 orders of magnitude to $92 \pm 27 \text{ S cm}^{-1}$, similar to results published for highly conductive MoS_2 films (100 S cm^{-1}).²⁰

In summary, a high-yielding synthesis of colloidal 2H- WSe_2 nanosheets was reported, which were shown to be phase pure by XRD. Preferential sheet alignment along the [001] direction upon solution casting was reflected in the XRD pattern and the correspondingly high conductivity values of the resulting thin films. Two-point conductivity measurements for unannealed and annealed devices gave an average value of 0.6 and 92 S cm^{-1} , respectively. Future work will focus on examining the viability of this material for use in solution-processed, nanosheet-based devices.

■ ASSOCIATED CONTENT

📄 Supporting Information

Experimental details, TGA/DSC, EDX, Raman spectra, and additional TEM and SAED images of unannealed WSe_2 . This material is available free of charge via the Internet at <http://pubs.acs.org>.

■ AUTHOR INFORMATION

Corresponding Author

*E-mail: brutchey@usc.edu.

Notes

The authors declare no competing financial interest.

■ ACKNOWLEDGMENTS

This work is supported by the National Science Foundation under DMR-1205712. P.D.A. acknowledges the National Science Foundation for a Graduate Research Fellowship and R.L.B. acknowledges the Research Corporation for Science Advancement for a Cottrell Scholar Award. The authors thank P. Erwin and S. Rodney (Thompson lab), J. Liu (Zhou lab), H. Mahalingam (Steier lab), Dr. E. Couderc (Bradforth/Brutchey lab), C. Beier (Brutchey lab), and Dr. F. Rabuffetti (Brutchey lab) for both experimental assistance and helpful discussions.

■ REFERENCES

(1) (a) Chen, J.; Kuriyama, N.; Yuan, H.; Takeshita, H. T.; Sakai, T. *J. Am. Chem. Soc.* **2001**, *123*, 11813. (b) Zhang, Y.; Ye, J.; Matsushashi, Y.; Iwasa, Y. *Nano Lett.* **2012**, *12*, 1136. (c) Chhowalla, M.; Amaratunga, G. A. *J. Nature* **2000**, *407*, 164. (d) Lauritsen, J. V.; Bollinger, M. V.; Laegsgaard, E.; Jacobsen, K. W.; Norskov, J. K.; Clausen, B. S.; Topsoe, H.; Besenbacher, F. *J. Catal.* **2004**, *221*, 510. (e) Justin, P.; Rao, G. R. *Int. J. Hydrogen Energy* **2010**, *35*, 9709. (f) Dominko, R.; Arcon, D.; Mrzel, A.; Zorko, A.; Cevc, P.; Venturini, P.; Gaberscek, M.; Remskar, M.; Mihailovic, D. *Adv. Mater.* **2002**, *14*, 1531. (g) Xiao, J.;

Choi, D.; Cosimbescu, L.; Koech, P.; Liu, J.; Lemmon, J. P. *Chem. Mater.* **2010**, *22*, 4522. (h) Thomalla, M.; Tributsch, H. *J. Phys. Chem. B* **2006**, *110*, 12167.

(2) (a) Morris, R. C.; Bhandari, R.; Coleman, R. V. *Phys. Rev. B* **1972**, *5*, 895. (b) Dunnill, C. W.; Edwards, H. K.; Brown, P. D.; Gregory, D. H. *Angew. Chem., Int. Ed.* **2006**, *45*, 7060.

(3) Goodson, K. E. *Science* **2007**, *315*, 342.

(4) Dominko, R.; Gaberscek, M.; Arcon, D.; Mrzel, A.; Remskar, M.; Mihailovic, D.; Pejovnik, S.; Jamnik, J. *Electrochim. Acta* **2003**, *48*, 3079.

(5) (a) Kumar, A.; Ahluwalia, P. K. *Eur. Phys. J. B* **2012**, *85*, 186. (b) Mak, K. F.; Lee, C.; Hone, J.; Shan, J.; Heinz, T. F. *Phys. Rev. Lett.* **2010**, *105*, 136805. (c) Wang, Q. H.; Kalantar-Zadeh, K.; Kis, A.; Coleman, J. N.; Strano, M. S. *Nat. Nanotechnol.* **2012**, *7*, 699.

(6) (a) Tributsch, H. *J. Electrochem. Soc.* **1978**, *125*, 1086. (b) Legma, J. B.; Vacquier, G.; Traore, H.; Casalot, A. *Mater. Sci. Eng., B* **1991**, *8*, 167.

(7) Kam, K. K.; Parkinson, B. A. *J. Phys. Chem.* **1982**, *86*, 463.

(8) Prasad, G.; Srivastava, O. N. *J. Phys. D Appl. Phys.* **1988**, *21*, 1028.

(9) (a) Agarwal, M. K.; Patel, P. D.; Vijayan, O. *Phys. Status Solidi A* **1983**, *78*, 133. (b) El-Mahalawy, S. H.; Evans, B. L. *Phys. Status Solidi B* **1977**, *79*, 713.

(10) Gamble, F. R. *J. Solid State Chem.* **1974**, *9*, 358.

(11) Bromley, R. A.; Yoffe, A. D.; Murray, R. B. *J. Phys. C: Solid State Phys.* **1972**, *5*, 759.

(12) (a) Pouzet, J.; Bernede, J. C.; Khellil, A.; Essaidi, H.; Benhida, S. *Thin Solid Films* **1992**, *208*, 252. (b) Legma, J. B.; Vacquier, G.; Casalot, A. *J. Cryst. Growth* **1993**, *130*, 253. (c) McKone, J. R.; Pieterick, A. P.; Gray, H. B.; Lewis, N. S. *J. Am. Chem. Soc.* **2013**, *135*, 223. (d) Benhida, S.; Bernede, J. C.; Delphine, S. M.; Jayachandran, M.; Sanjeeviraja, C. *Mater. Chem. Phys.* **2003**, *81*, 78. (e) Delphine, S. M.; Jayachandran, M.; Sanjeeviraja, C. *Mater. Chem. Phys.* **2003**, *81*, 78. (13) Huang, J. M.; Kelley, D. F. *Chem. Mater.* **2000**, *12*, 2825.

(14) Duphil, D.; Bastide, S.; Rouchaud, J. C.; Pastol, J. L.; Legendrel, B.; Levy-Clement, C. *Nanotechnology* **2004**, *15*, 828.

(15) (a) Franzman, M. A.; Perez, V.; Brutchey, R. L. *J. Phys. Chem. C* **2009**, *113*, 630. (b) Webber, D. H.; Brutchey, R. L. *Chem. Commun.* **2009**, 5701. (c) Norako, M. E.; Brutchey, R. L. *Chem. Mater.* **2010**, *22*, 1613. (d) Webber, D. H.; Brutchey, R. L. *Inorg. Chem.* **2011**, *50*, 723. (e) Norako, M. E.; Greaney, M. J.; Brutchey, R. L. *J. Am. Chem. Soc.* **2012**, *134*, 23. (f) Buckley, J. J.; Rabuffetti, F. A.; Hinton, H. L.; Brutchey, R. L. *Chem. Mater.* **2012**, *24*, 3514.

(16) Kurth, D. G.; Lehmann, P.; Lesser, C. *Chem. Commun.* **2000**, 949.

(17) Wong-Ng, W.; McMurdie, H.; Paretzkin, B.; Zhang, Y.; Davis, K.; Hubbard, C.; Alan, D.; Stewart, J. *Powder Diffr.* **1987**, *2*, 257.

(18) Mead, D. G.; Irwin, J. C. *Can. J. Phys.* **1977**, *55*, 379.

(19) Galun, E.; Cohen, H.; Margulis, L.; Vilan, A.; Tsirlina, T.; Hodes, G.; Tenne, R.; Hershinkel, M.; Jaegermann, W.; Ellmer, K. *Appl. Phys. Lett.* **1995**, *67*, 3474.

(20) Tachibana, H.; Yamanaka, Y.; Sakai, H.; Abe, M.; Matsumoto, M. *Chem. Mater.* **2000**, *12*, 854.